P. BISWAS*, R. BHANDARI**, M. KUMAR MONDAL*#, D. MANDAL*

EFFECT OF MICROSTRUCTURAL MORPHOLOGY ON MICROSCALE DEFORMATION BEHAVIOR
OF Al-4.5Cu-2Mg ALLOY

The microscale deformation behaviour of the Al-4.5Cu-2Mg alloy has been studied to understand the influence of various processing routes and conditions, i.e. the gravity casting with and without grain refiner, the rheocast process and the strain induced melt activation (SIMA) process. The micromechanics based simulations have been carried out on the optical microstructures of the alloy by 2D representative volume elements (RVEs) employing two different boundary conditions. Microstructural morphology, such as the grain size, the shape and the volume fraction of α-Al and binary eutectic phases have a significant effect on the stress and strain distribution and the plastic strain localization of the alloy. It is found that the stress and strain distribution became more uniform with increasing the globularity of the α-Al grain and the α-Al phase volume fraction. The simulated RVEs also reveals that the eutectic phase carries more load, but least ductility with respect to the α-Al phase. The SIMA processed alloy contains more uniform stress distribution with less stress localization which ensures better mechanical property than the gravity cast, grain refined and rheocast alloy.

Keywords: Al-4.5Cu-2Mg Alloys, Optical Microstructure, Representative Volume Element (RVE), Finite Element Method, Microscale deformation

1. Introduction

The micromechanical computational modelling has gained broad research interest in the field of material science and engineering as the real-life problem can solve easily. The computational modelling is a historical invention and it reduces time, large sets of experiment and investment cost [1]. In recent time, the computational modelling of the microstructure is a popular field of materials research to understand the effect of the microstructural features such as the size, shape, orientation and the volume fraction of different phases on the micromechanical response of materials. Although those microstructural features are measured in different length scale ranging from nanometers to micrometres, there is an inherent correlation between them [2].

Few available research works have been reported on micromechanical modelling of approximate representative volume elements (RVEs). In a previous study, Ganesh and Chawla [3] investigated the microlevel deformation behaviour of metal matrix composite using an image processing software 'Raster-Vect' to vectorize the scanning electron microscopy images of the composite by ABAQUS finite element software. Previously, Paul [4] also simulated the deformation behaviour of dual phase steel using ABAQUS software. It was reported that plastic strain localization occurred because of the differences in deformation between the soft (ferrite) and the hard (martensite) phase. In another study, Hossein et al. Al [5] predicted the deformation and failure behaviour of dual phase (DP) steel using the finite element analysis and report that localized shear strain and stress concentrated area as the failure initiation point in the DP steel. Later, Sirinakorn et al. [6] employed the Gurson-Tvergaard-Needleman (GTN) model to investigate the effect of various microstructure constituents and characteristics on deformation, flow and fracture behaviour of DP high strength steel using representative volume elements (RVEs) model and analyze the damage initiation for the DP steel. Moreover, Pheltam et al. [7] generated the 2D RVEs of tempered steel to study the stress-strain responses using both the macro and micro level simulation. Further, the authors investigated the effect of carbide characteristic on DP steel in terms of stress and strain distribution in the tempered steel and found that at a low temperature and high holding time tempered steel has a higher stress concentration at the local circumference of carbide. Additionally, Ramazani et al. [8] used an extended finite element method (XFEM) for simulating martensite cracking of DP steel RVE models to find out the failure initiation point at mesoscale also the failure initiation behaviour and stress-state-dependent plasticity was forecasted by Wu et al. [9]. In a recent investigation Paul et al. [10] determined the bulk flow properties of DP 780 and DP 590 steels from constituent phases flow properties using FE based micromechanics modelling of approximated 3D RVEs.

* NATIONAL INSTITUTE OF TECHNOLOGY, DEPARTMENT OF METALLURGICAL AND MATERIALS ENGINEERING, DURGAPUR-713209, INDIA
** BIRBHUM INSTITUTE OF ENGINEERING AND TECHNOLOGY, DEPARTMENT OF MECHANICAL ENGINEERING

\# Corresponding author: manas.nitdgp@gmail.com

However, most of the previous research work on micromechanics are based on dual phase steel and some work on alloys and composites [11-14]. Those works are mainly based on approximate RVEs which is not able to show the actual mechanical response of actual microstructural morphology.

However, there are several processes such as the addition of grain refining elements, semi solid processing, spray casting, and rapid cooling are used to obtain improved mechanical properties of materials [15-17]. Among the semi solid processes rheocast and SIMA process are the most popular. In rheocasting process [18], the semi-solid slurry is prepared by stirring, but rheocast alloy has porosity and segregation problem. It can be effectively reduced by SIMA process [19] because this process combines both the casting and rolling process. In the SIMA process, the required microstructural morphology of alloys can obtained by deformation with subsequent heat treatment in the mushy zone [20-21]. Furthermore, SIMA is a budding technology with the various commercial merits such as simplicity and minimum setup cost and it can be apply to most engineering alloys, including aluminum, copper, magnesium and ferrous alloys [22-24]. In the present work, Al-4.5Cu-2Mg alloy has been synthesized by gravity casting process with and without grain refiner and rheocasting process. Further, the SIMA process has been performed on the gravity cast with out grain refined alloy.

The Al-Mg-Cu alloy has gained great research interest due to improved mechanical properties that include good weight to strength ratio, high strength, low coefficient of thermal expansion, good castability, reliable formability and hardenability [25-27]. The effect of various processing routes and conditions 'in terms of size and shape of the α-Al grain and volume fraction of different phases' on the micro mechanical response of the alloy has been studied using optical microstructures RVE model employing two different boundary conditions.

2. Experimental procedure

In this work, commercially pure aluminium (99.7%), magnesium (99.95%), copper (99.95%) and Al-5Ti-1B master alloy were used to develop Al-4.5Cu-2Mg alloy with and without grain refiner (Al-5Ti-1B) by gravity casting method. The small blocks of commercially pure aluminium were melted at 720°C temperature in a 3 kg capacity clay graphite crucible using a heat resistance furnace under inert gas (argon) atmosphere. Thereafter, aluminium foil wrapped copper was added to the melt and the melt was stirred for 2-3 mins. After complete dissolution of Cu, magnesium wrapped with aluminium foil was added into the melt. Then the Al-5Ti-1B master alloy was added into the melt and hold for 10 minutes for complete dissolution of the master alloy. Subsequently, hexachloroethane (1 wt. %) was added into the melt for removal of dissolved gases. Afterward, the molten alloy was immediately poured into a preheated (≈250°C) permanent cast iron mold.

In the rheocasting process, the melt was taken out from the furnace and slag was removed. Then, the melt was stirred with a mechanical stirrer at around 300 rpm for 10 minutes by maintaining approximately isothermal condition (615°C). Thereafter, the semi-solid melt was poured into a preheated (400°C) permanent cast iron mould and it was allowed to cool to room temperature.

In the SIMA process, the gravity cast alloy was homogenized at 460°C for 6 hrs. After homogenization, the samples were forged at 460°C to reduce the thickness about 50% followed by air cooling. Thereafter, the samples were preheated at 280°C for 1 hrs. Subsequently, 50% deformation at below the recrystallization temperature of the alloy was applied to the samples in a four high warm rolling mill (250 mm roll diameter with and 300 mm barrel length). Furthermore, the different processing route and their abbreviation are represented in Table 1.

TABLE 1

Abbreviation used for different processing route and condition for synthesis of Al-4.5Cu-2Mg alloy

Sl. No.	Process	Process abbreviation
1	Gravity cast	**P₁**
2	Gravity cast with grain Refiner	**P₂**
3	Rheocast	**P₃**
4	SIMA process	**P₄**

Metallography samples were polished by standard procedure and etched by Keller's reagent solution. Thereafter, the evaluation of different phases was investigated under an optical microscope (Leica DM 2500). The Vickers micro hardness tester (Model-UH3, Reicherter and Stiefelmayer) was used to measure the microhardness of different phases at 50 gmf load. The tensile specimens were prepared as per ASTM E8M standard and tensile testing was carried out using computer controlled 50T Instron (Instron-8501) at room temperature with a strain rate of 10^{-3} s^{-1}.

3. Constitutive description

The elastic-plastic behaviour of the alloy has been evaluated using Ramberg-Osgood model [28]. The ramberg-osgood relation is a polynomial expression, which can be represented by the equation (1).

$$E\varepsilon = \sigma + \alpha\left(\frac{\pm\sigma}{\sigma_0}\right)^{n-1}\sigma \qquad (1)$$

Where, σ, ε, E α and n (>1) are nominal stress, nominal strain, young's modulus, yield offset and strain hardening exponent (non-linear term) respectively for plastic deformation.

Strain energy density has been calculated using equation (2).

$$W = \int\sigma d\varepsilon \qquad (2)$$

Equation (1) has been solved using Newton's method by considering $q = \pm\sigma$ with an initial guess $\sigma = E|\varepsilon|$ if $E|\varepsilon| \leq \sigma_0$ and $\sigma = \pm\left[E|\varepsilon|\sigma_0^{n-1}/\alpha\right]^{\frac{1}{n}}$ if $E|\varepsilon| \rangle \sigma_0$ for getting the value of stress. The s is corrected as c_σ nand the Newton equation of the equation (1) can be expressed by equation (3).

$$\left[1+n\alpha\left(\frac{q}{\sigma_0}\right)^{n-1}\right]c_\sigma = E\varepsilon - \sigma - \alpha\left(\frac{q}{\sigma_0}\right)^{n-1}\sigma \tag{3}$$

$$\sigma = \sigma - c_\sigma \tag{4}$$

In this case, the material stiffness matrix is given as:

$$\frac{\partial\sigma}{\partial\varepsilon} = \frac{E}{1+n\sigma(q/\sigma_0)^{n-1}} \tag{5}$$

The plastic flow stress of the α-Al and the eutectic phase is expressed by equation (6) and (7) under loading.

$$\sigma = \sigma_{y,Al} + K_{Al}\varepsilon_{ep}^{n_{Al}} \tag{6}$$

$$\sigma = \sigma_{y,Eu} + K_{Eu}\varepsilon_{ep}^{n_{Eu}} \tag{7}$$

Where, $\sigma_{y,Al}$ and $\sigma_{y,Eu}$ are the initial yield strength of primary α-Al and eutectic phase, K_{Al} and K_{Eu} are hardening coefficient and n_{Al} and n_{Cu} are the strain hardening exponent of primary α-Al and eutectic phase, respectively.

4. Pre-modeling

The optical microstructures of the alloy have been used to develop two-dimensional (2D) RVEs. Raster images are vectorized using Vextractor, an image analysis software and the vectorized RVE (0.45×0.45 mm^2) is shown in Figure 1. The microscale deformation behaviour of the alloy has been simulated by considering two different types of boundary conditions shown in Figure 2.
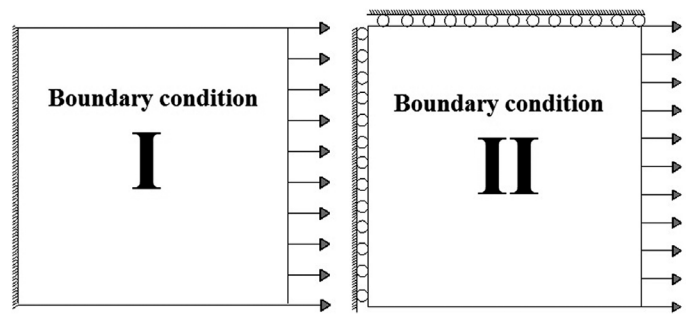
Fig. 2. Case-I and -II boundary conditions used for modelling

The bulk hardness (H) of the alloy is calculated using the rule of mixture method and the bulk hardness expression can be represented by the equation (8).

$$H = V_P H_P + V_E H_E \tag{8}$$

Where V_P and V_E are volume fraction, H_P and H_E are the micro-hardness of the primary α-Al phase and Cu-rich eutectic phase, respectively, and subscript P and E denote the primary phase and the eutectic phase respectively. The micro-hardness and volume fraction of individual phases and bulk hardness are shown in Table 2.

TABLE 2

Calculated volume fraction of phases and their corresponding hardness (VHN) and calculated bulk hardness (VHN) of Al-4.5Cu-2Mg alloy at different process condition

Process	V_P	H_P	V_E	H_E	H
P_1	0.81	69	0.19	81	71
P_2	0.51	72	0.49	90	80
P_3	0.67	94	0.33	108	96
P_4	0.82	111	0.18	120	113

An equation has been developed by considering a first-order polynomial fitting between the yield strength and microhardness of the alloy to get the approximate yield strength of the individual phases (Fig. 3). The developed equation is given as:
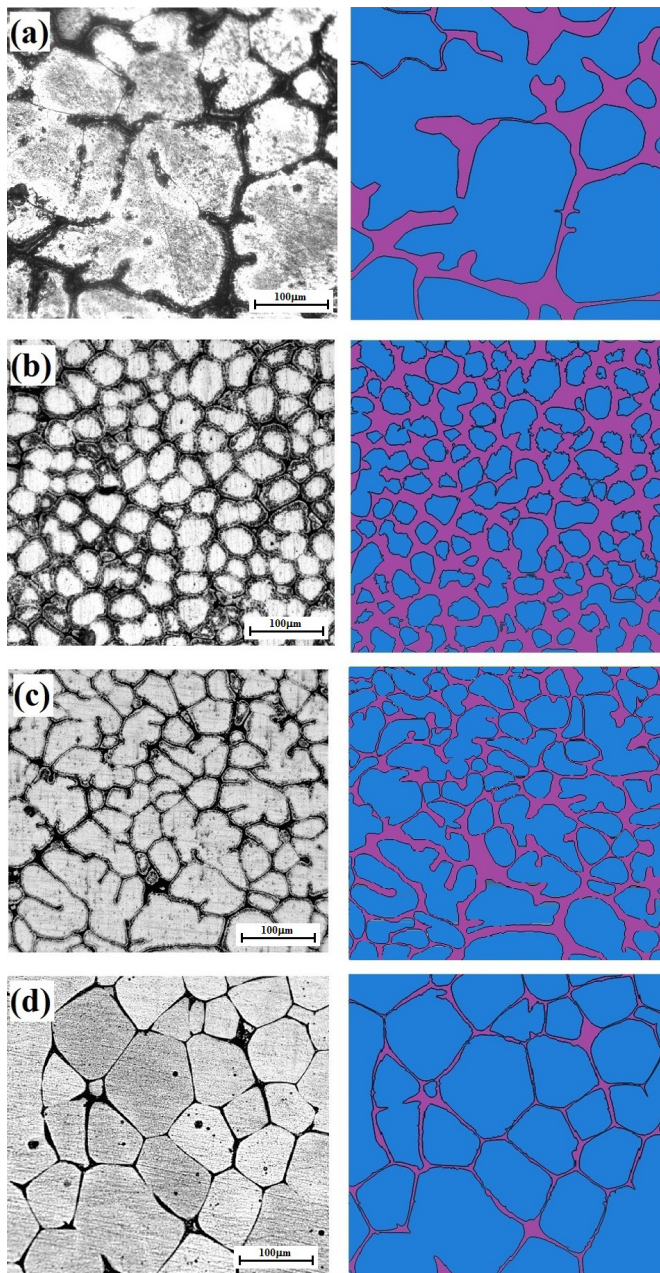

Fig. 1. Optical microstructures and vectorized RVEs: (a) Gravity cast (P_1) (b) gravity cast with grain refiner (P_2) (c) Rheocast (P_3) and (d) SIMA process (P_4)

$$Y = -68.65789 + 2.53509X \qquad (9)$$

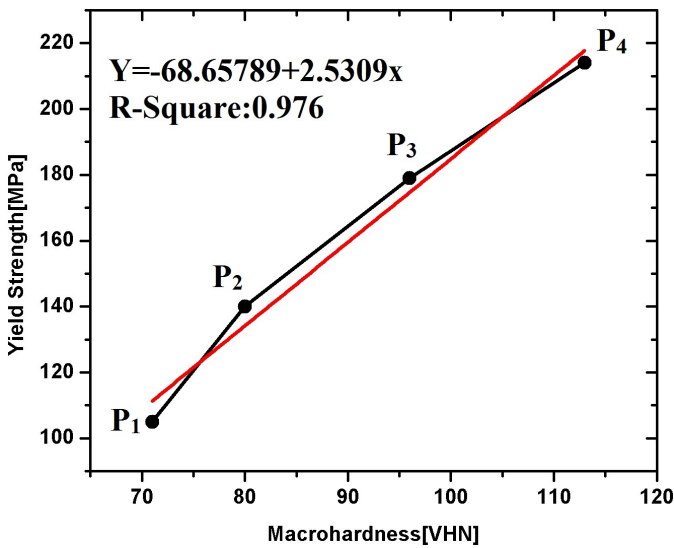Where Y and X are the yield strength and the microhardness of the individual phase.

Fig. 3. Curve fitting for calculation of phase's yield strength using bulk hardness (VHN)

The calculated yield strength of the individual phases is stated in Table 3.

TABLE 3

The estimated yield strength of α-Al and eutectic phase

	Yield Strength [MPa]	
Route	α-Al Phase	Eutectic Phase
P_1	105	139
P_2	114	160
P_3	144	235
P_4	213	236

5. Result and discussions

The optical microstructures of Al-4.5Cu-2Mg alloy, processed through different routes and condition are shown in Figure 1a-d. The optical microstructure of gravity cast (P_1) alloy (Fig. 1a) reveals the presence of coarse dendritic α-Al phase and non-uniform thicker eutectic phase, whereas the grain refined gravity cast alloy (P_2) has fine and nearly globular α-Al grain (Fig. 1b) with uniformly distributed eutectic network. Furthermore, the volume fraction of eutectic phase is increased from 0.19 to 0.49. The optical microstructure of rheocast alloy (P_3) exhibits both the dendritic and non-dendritic α-Al grains with thin eutectic network and the volume fraction of eutectic phase is decreased to 0.33 (Fig. 1c) with respect to the grain refined alloy. Finally, the optical microstructure of SIMA processed alloy (P_4) (Fig. 1d) has the globular α-Al grains and uniformly distributed thinner eutectic network with a minimum volume fraction of the eutectic phase (0.18). However, the dendritic structure forms as a result of slow cooling and directional solidification. The addition of grain refiner (Al-Ti-B master alloy), modifies the dendritic structure to an equiaxed morphology because the grain refiner reduces the surface energy of atoms and restrict the growth of the grains as well as the refiner acts as a nucleation site of α-Al grains. In the rheocast process, dendritic structures finally break into equiaxed structure caused by the shearing action of the mechanical stirrer in the liquid melt. Moreover, in SIMA process, dendritic structures are modified into globular structures due to the warm deformation followed by heat treatment at messy zone as well as solute state diffusion of atoms. The combined effect of casting and forging minimize the micro porosity of the alloy. As a result of this the ultimate tensile strength, elongation and hardness are improved in SIMA processed alloy.

Fig. 4 shows the Von Mises stress distribution in simulated RVEs (P_1, P_2, P_3 and P_4) employing case I boundary condition at various strain levels (Table 4). The Von Mises stress distribution and its density varies with the change in the process route and condition. The simulated RVE of gravity cast alloy has less induced Von Mises stress compare to other processed alloy RVEs. It is found that the Von Mises stress distribution is non-uniform and the Von Mises stress localization is occurring in the narrow eutectic phase region. Those stress localized regions generally act as a crack initiation point followed by final failure of the material. Moreover, the load carrying capacity of the primary α-Al and eutectic phase are different and the induced Von Mises stress is higher in eutectic phase than the primary α-Al phase (Fig. 4a). The grain refined gravity cast alloy exhibits a better Von Mises stress distribution with respect to simple gravity cast alloy. A clear uniformity in Von Mises stress distribution is found in the primary α-Al phase as well as eutectic phase (Fig. 4b) as the dendritic α-Al grains change into the equiaxed α-Al. The overall load distribution becomes non-uniform in the alloy due to the presence of a thicker eutectic network. As that thicker eutectic network carries the maximum applied load and it protects to deform as a result of it stress localization occurs at the α-Al and eutectic phase interface. Therefore, the overall elongation of the alloy decreases as the bonding of α-Al and eutectic phase or interface become poor and shear failure occurs. Moreover, the stress localized region occurs at the sharp corners or tips of the eutectic phase, where voids and cracks initiation arise. The rheocast alloy (Fig. 4c) has a uniform stress distribution in the α-Al phase and eutectic phase with some stress localized region because its microstructure contains a combination of equiaxed and globular α-Al grains and very few α-Al grains with sharp corners. Furthermore, the difference of induced Von Mises stress is less due to the lower volume fraction of the thinner eutectic phase which is uniformly distributed throughout the microstructure (RVEs). Finally, SIMA processed alloy (Fig. 4d) exhibits the presence of a uniform Von Mises stress distribution in both the phases and induced stress difference among the phases is insignificant because it has more uniformly distributed globular α-Al grains as well as very thin and uniform eutectic network.
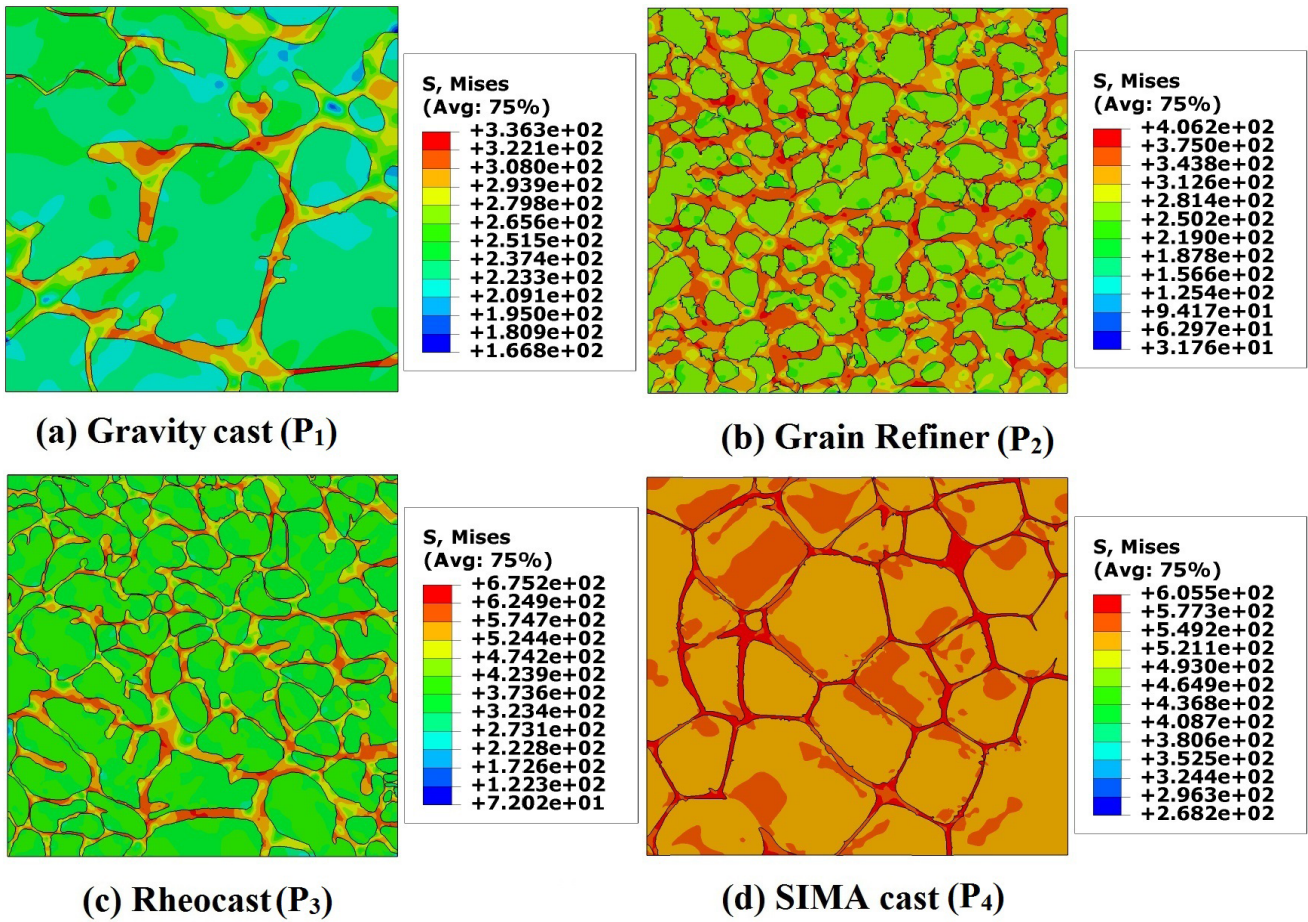
(a) Gravity cast (P₁)

(b) Grain Refiner (P₂)

(c) Rheocast (P₃)

(d) SIMA cast (P₄)

Fig. 4. Von Mises stress distribution at different strain level using case-I boundary condition

(a) Gravity die cast
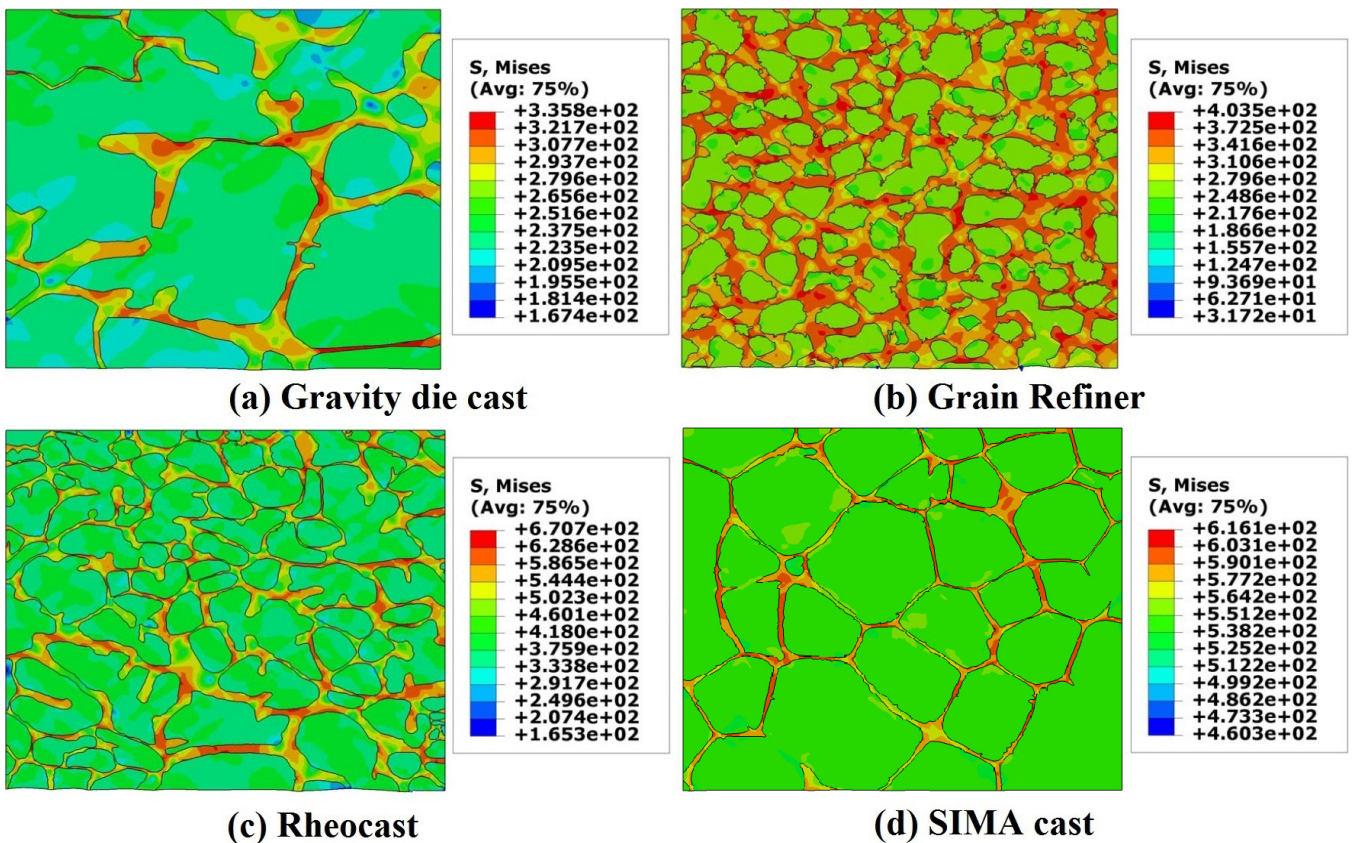
(b) Grain Refiner

(c) Rheocast

(d) SIMA cast

Fig. 5. Von Mises distribution at different strain level using case-II boundary condition

Strain level (% El) of Al-4.5Cu-2Mg alloy in different
process conditions

Condition	P_1	P_2	P_3	P_4
Strain level (% El)	1.00	1.27	4.80	7.30

The Von Mises stress distribution of different simulated RVEs (P_1, P_2, P_3 and P_4), employing case-II boundary condition at various strain levels (Table 4) are shown in Fig. 5. It is evident from Fig. 4 and Fig. 5 that the simulated RVEs under both the boundary condition (Case-I and Case-II) have similar stress distribution. It is found that the higher load is carried by eutectic phase, whereas localized yielding occurs in primary α-Al phase (Fig. 5).The induced stress density is more in eutectic phase with respect to α-Al phase. The stress concentration region is minimum in the P_3 and P_4 with respect to the P_1 and P_2. Therefore, there is a chance of catastrophic failure is more in the P_1 and P_2. The P_4 will show more ductility due to uniform stress distribution in α-Al and eutectic phase as well as a minimum induced stress difference between the phases.

The equivalent plastic strain distribution in simulated RVEs of various process routes and condition under the uniaxial tensile load, employing case I boundary conditions with different strain level (Table 4) is shown in Fig. 6. It is found that the strain

originates at the fixed edge and subsequently, it spread through the RVEs in the direction of loading and there is a sharp difference between α-Al and eutectic phase strain values. The P_1 RVE (Fig. 6a) display the localized strain in α-Al phase. This strain localized region significantly reduces the overall ductility of the alloy and a void is formed and propagate which is the cause for the final failure. Therefore the alloy possessed through gravity cast route has relatively poor ductility and strength. The grain refined alloy (Fig. 6b) simulated RVE has a comparatively uniform distribution of strain due to the presence of fine equiaxed α-Al grains, but some strain localized region, as well as a huge difference of induced strain in between α-Al phase and eutectic phase is found. Hence, the ductility of the alloy became poor. Further, the rheocast alloy (Fig. 6c) has a slight improvement in strain distribution with respect to grain refined alloy. Because it has few globular α-Al grains and thinner and uniform eutectic network. As a result of it, induced strain difference between α-Al phase and eutectic phase is less. The strain distribution in SIMA processed alloy (Fig. 6d) is superior to other processed alloy because it has globular α-Al grains and uniformly distributed very thin eutectic network. The induced strain in α-Al and eutectic is also more or less uniform. Therefore, P_4 can possess better properties than the others.

Fig. 7 depicts multiple colour bands of equivalent plastic strain in different RVEs during the uniaxial tensile test at dif-
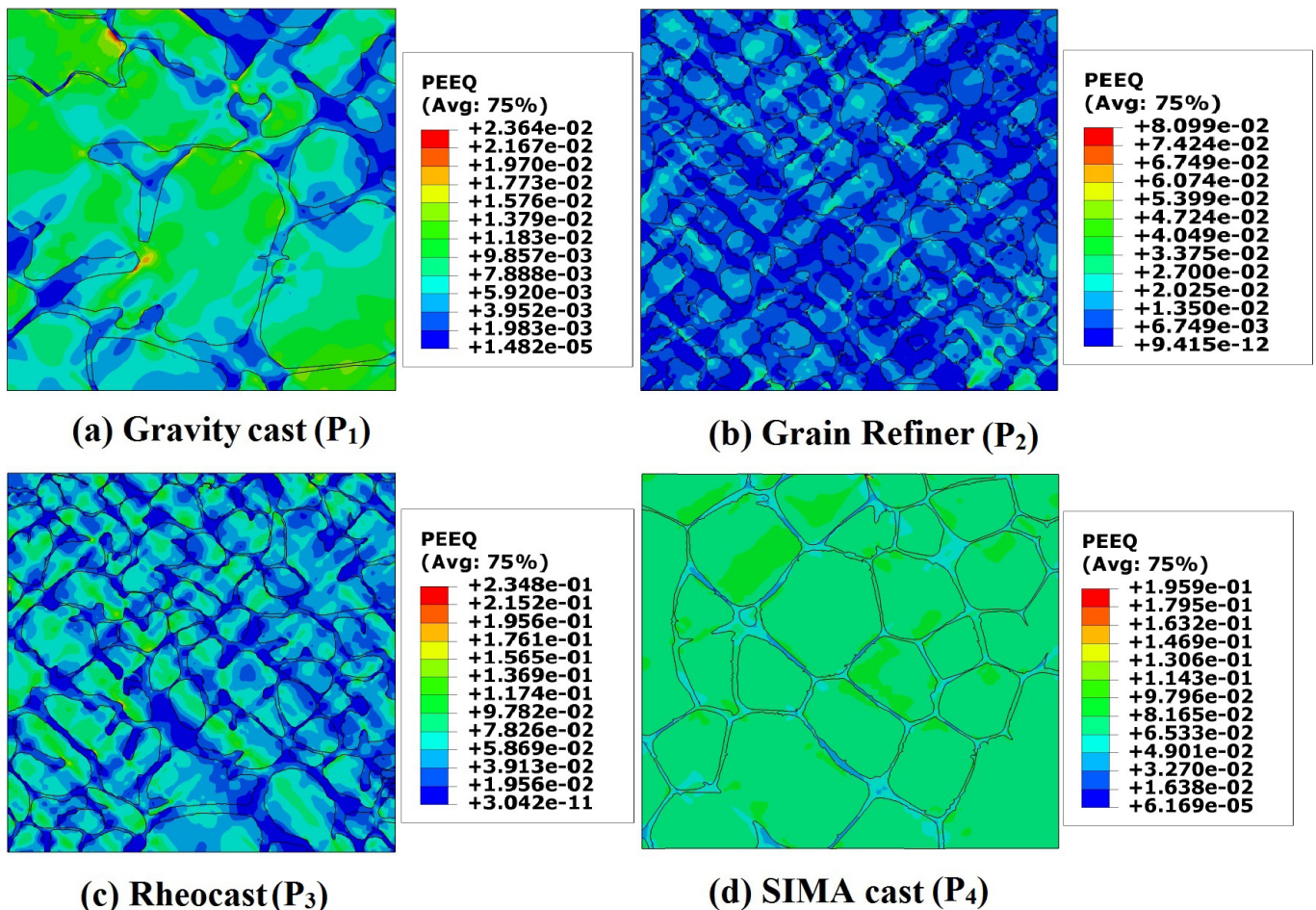

(a) Gravity cast (P_1)

(b) Grain Refiner (P_2)

(c) Rheocast (P_3)

(d) SIMA cast (P_4)

Fig. 6. Equivalent plastic Strain distribution at different strain level using case-I boundary condition

(a) Gravity die cast

(b) Grain Refiner
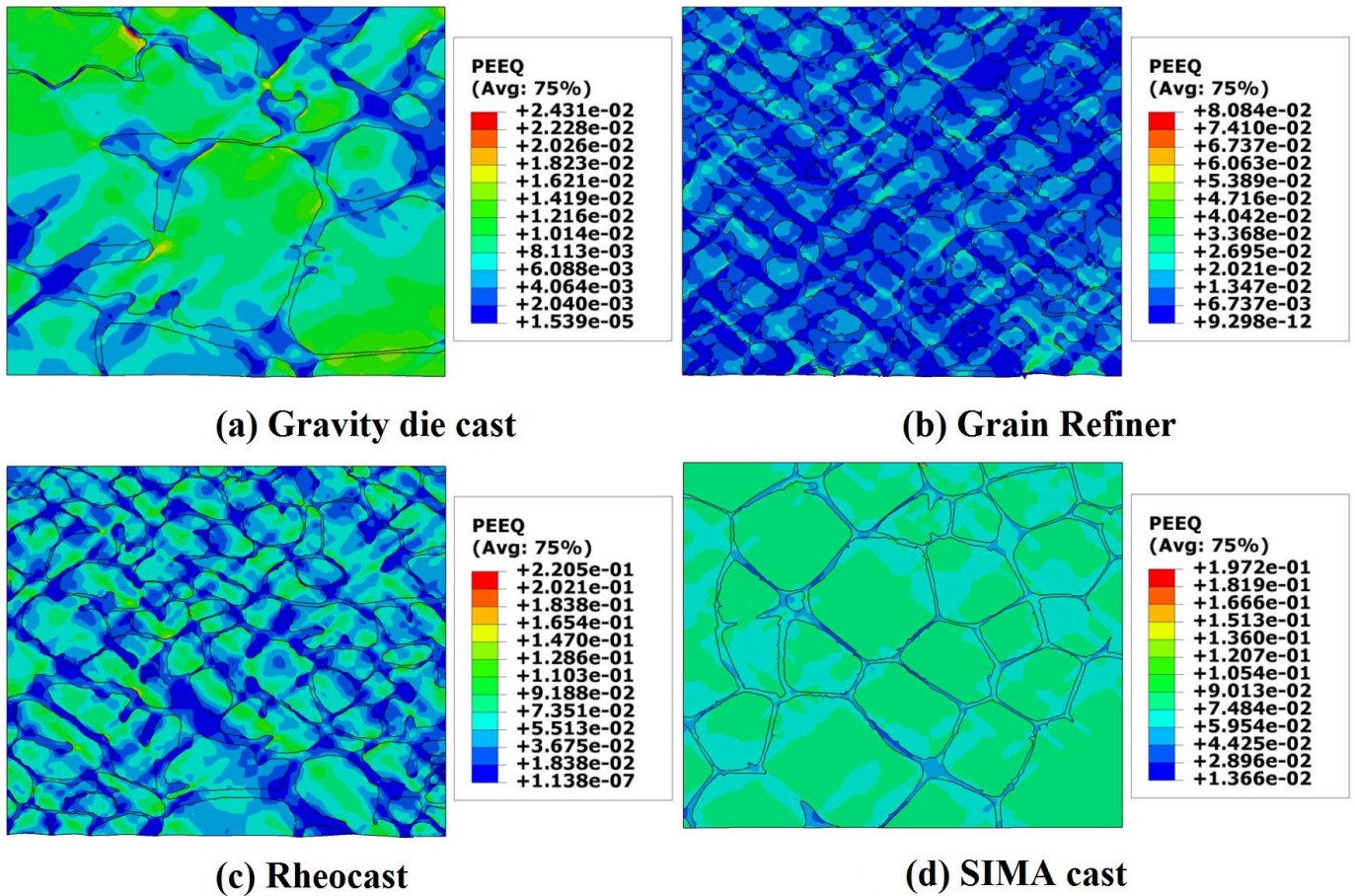
(c) Rheocast

(d) SIMA cast

Fig. 7. Equivalent plastic Strain distribution at different strain level using Case-II boundary condition

ferent strain level (Table 4) with case II boundary condition. The load is applied to the right side of RVEs and this load is transmitted to left side throughout the RVEs and initial strain localization arises at the top left side corner of RVEs due to the boundary condition. The induced strain is much higher in the primary phase with respect to eutectic phase (Fig. 7) as primary phase yield strength is much lower than the eutectic phase. The induced strain is decreased with decreasing volume fraction of primary α-Al phase or vice versa. The strain distribution in the simulated RVEs with case II boundary condition follows the same path of case-I boundary condition. In this case, also the induced strain distribution becomes uniform as globularity of primary α-Al phase is increased (Fig. 7a-d).

The principal stress (S11) distribution in different simulated RVEs at different strain level (Table 4) with case-I boundary condition is shown in Fig. 8. It is clear from Fig. 8 that the alloy processed through gravity casting route carries a minimum amount of principal stress, whereas the SIMA process alloy carries a maximum amount of principal stress. The P_1 and P_2 and P_3 processed alloy have non-uniform distribution of S11 stress with the stress localized region and the induced stress in eutectic phase is much higher and non-uniform with respect to α-Al phase, whereas in the SIMA processed alloy has uniform principal stress distribution and the induced principal stress is nearly same in both the phases. The stress localization is found to be occurring in the narrow eutectic phase region and at the

sharp corners of the simulated contour. The principle stress (S11) results also confirm that the globular α-Al grain and a thinner uniformly distributed eutectic network in the alloy provide a better mechanical response. The simulated RVEs (Fig. 9) with case-II boundary condition also shows the similar type of deformation behaviour of the alloy.

The true stress-strain plots of different RVEs in individual phases with the case I and case II boundary condition are presented in Fig. 10 and Fig. 11. It shows that the elongation of the primary phase is more than the eutectic phase in all cases as the primary α-Al phase is softer than the eutectic phase and the induced stress in the eutectic phase is much higher than the α-Al phase. Furthermore, it is clear from the Fig. 10 and Fig. 11 that the strength and elongation values of SIMA processed alloy is much higher than the other processed alloy.

Fig. 12 displays the displacement magnitude (U, Magnitude) of different RVEs under case-I boundary condition. Two closely situated nodes in the simulated RVEs at the high strain region (red zone) are shown in (Fig. 12a-d). The node number 7567 of gravity cast alloy is in the primary α-Al phase, whereas node number 518 is in eutectic phase which is attached to node 14227. The displacement magnitude of node 7567 is 0.00367 and node 518 is 0.00031. It clearly depicts that the displacements in the primary α-Al phase nodes are always greater than the eutectic phase, although the nodes are lying side by side of the primary and eutectic phase. Further, the displacement magnitude of two
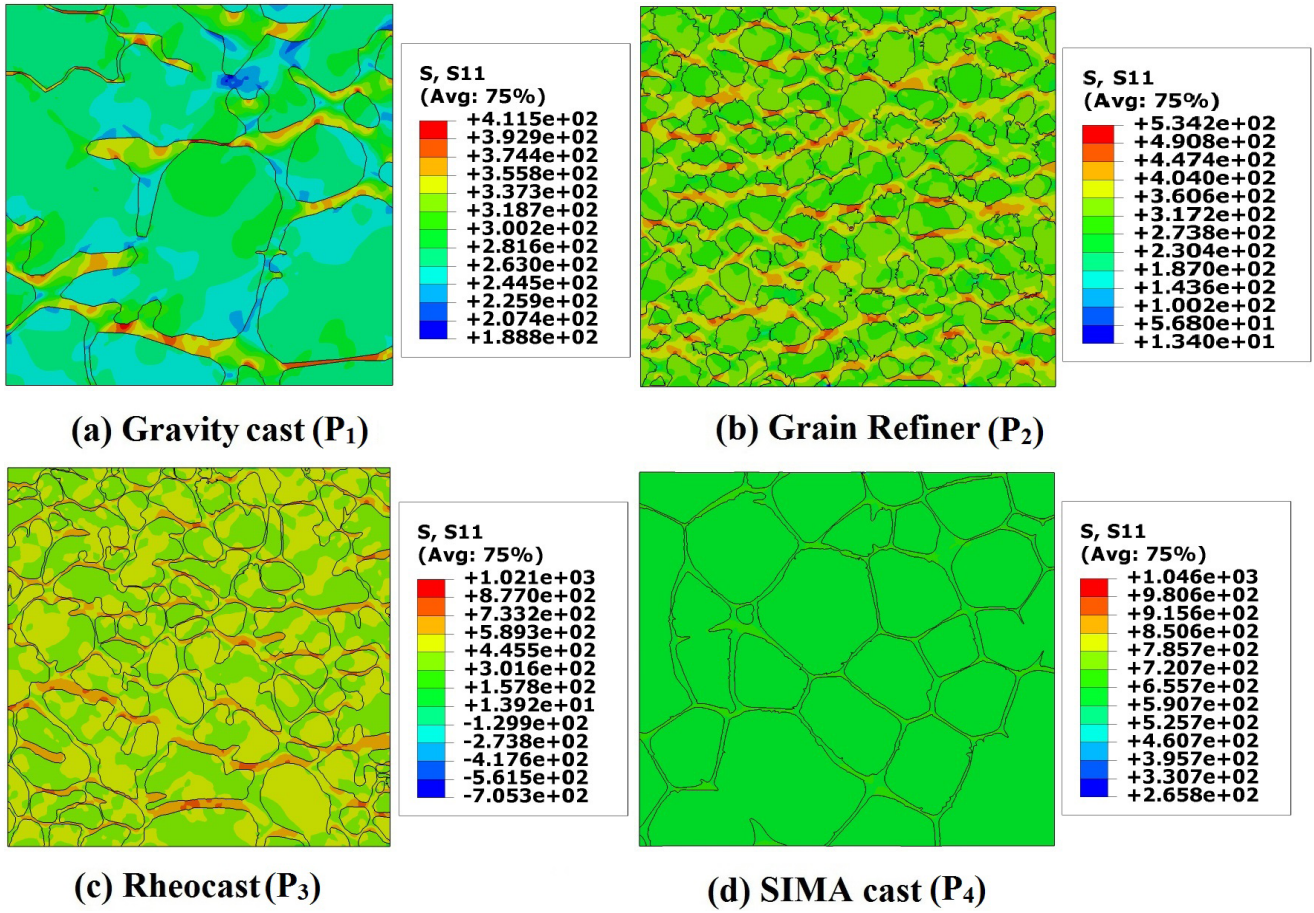
1582

(a) Gravity cast (P₁)

(b) Grain Refiner (P₂)

(c) Rheocast (P₃)

(d) SIMA cast (P₄)

Fig. 8. Nominal stress distribution at different strain level using case-I boundary condition

(a) Gravity die cast

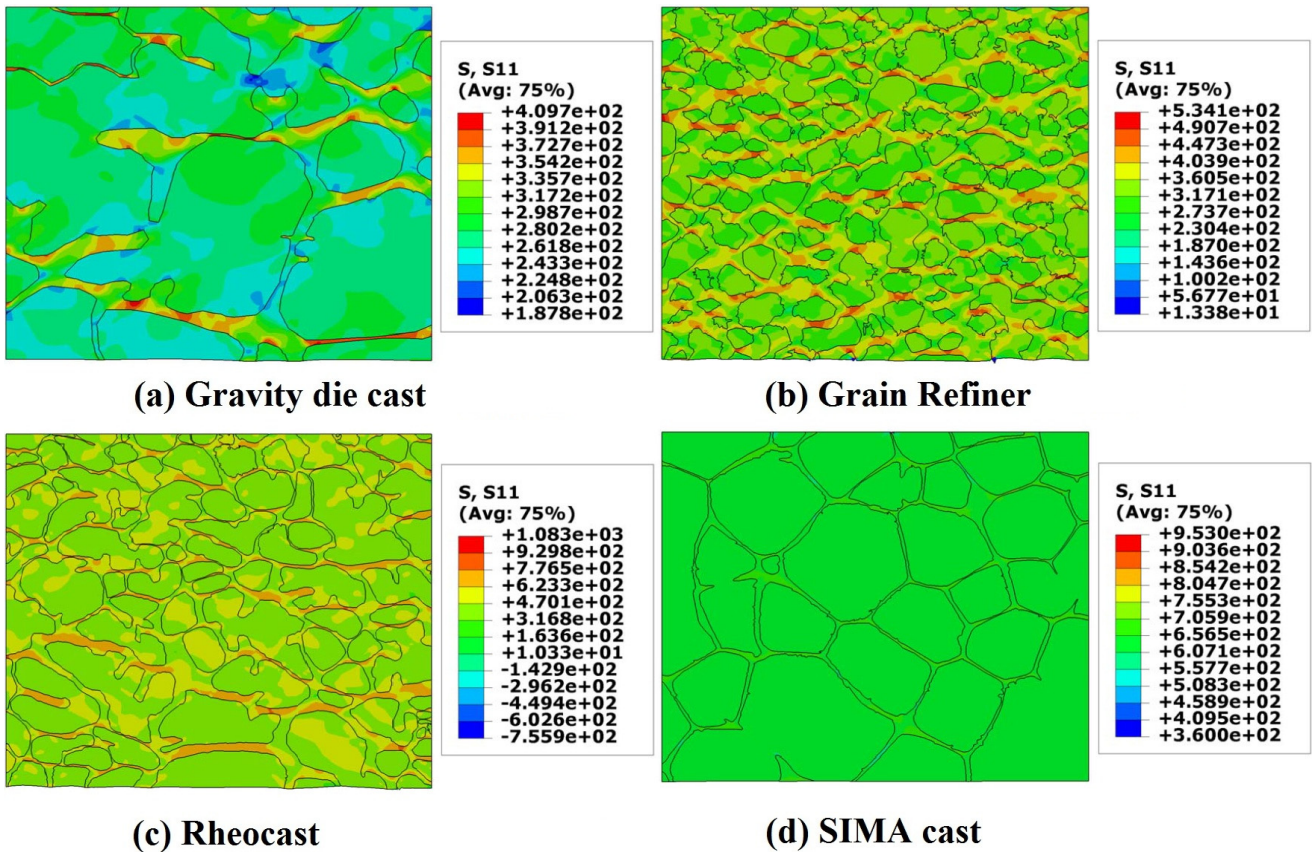**(b) Grain Refiner**

(c) Rheocast

(d) SIMA cast

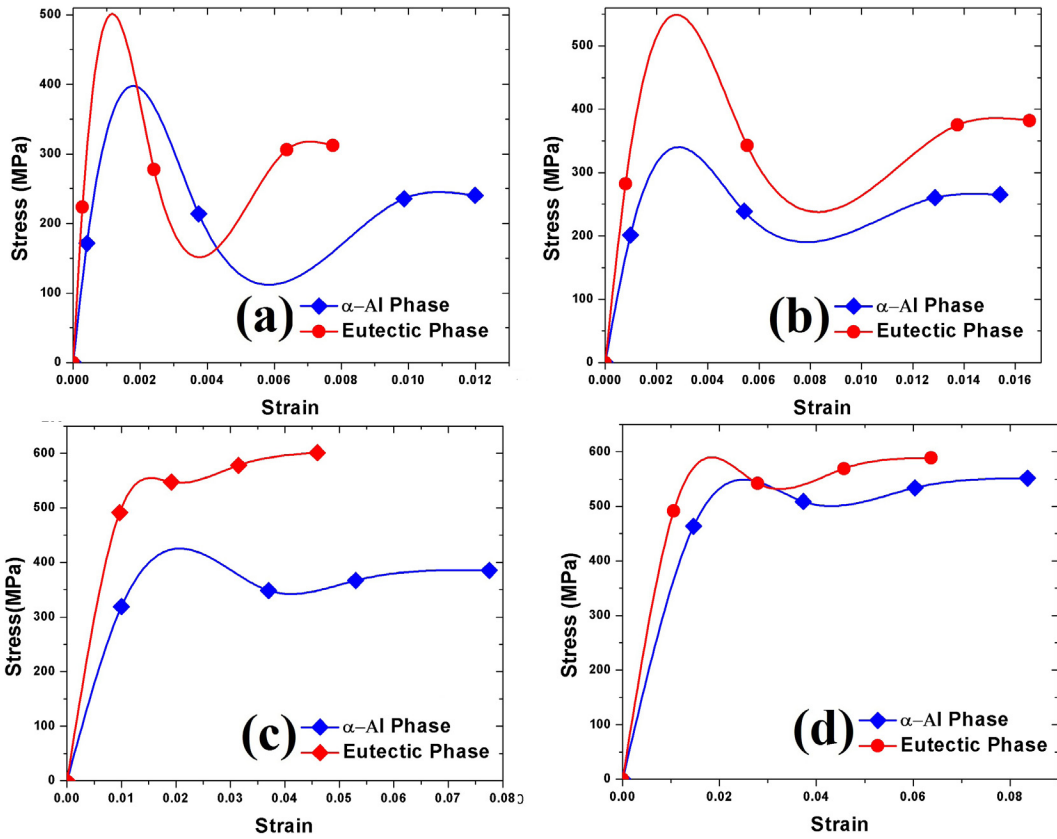Fig. 9. Nominal stress distribution at different strain level using Case-II boundary condition

Fig. 10. True stress vs. true strain plot of primary α-Al and eutectic phase employing case-I boundary condition: (a) Gravity cast (P_1) (b) Gravity cast with grain refiner (P_2) (c) Rheocast (P_3) (d) SIMA (P_4)

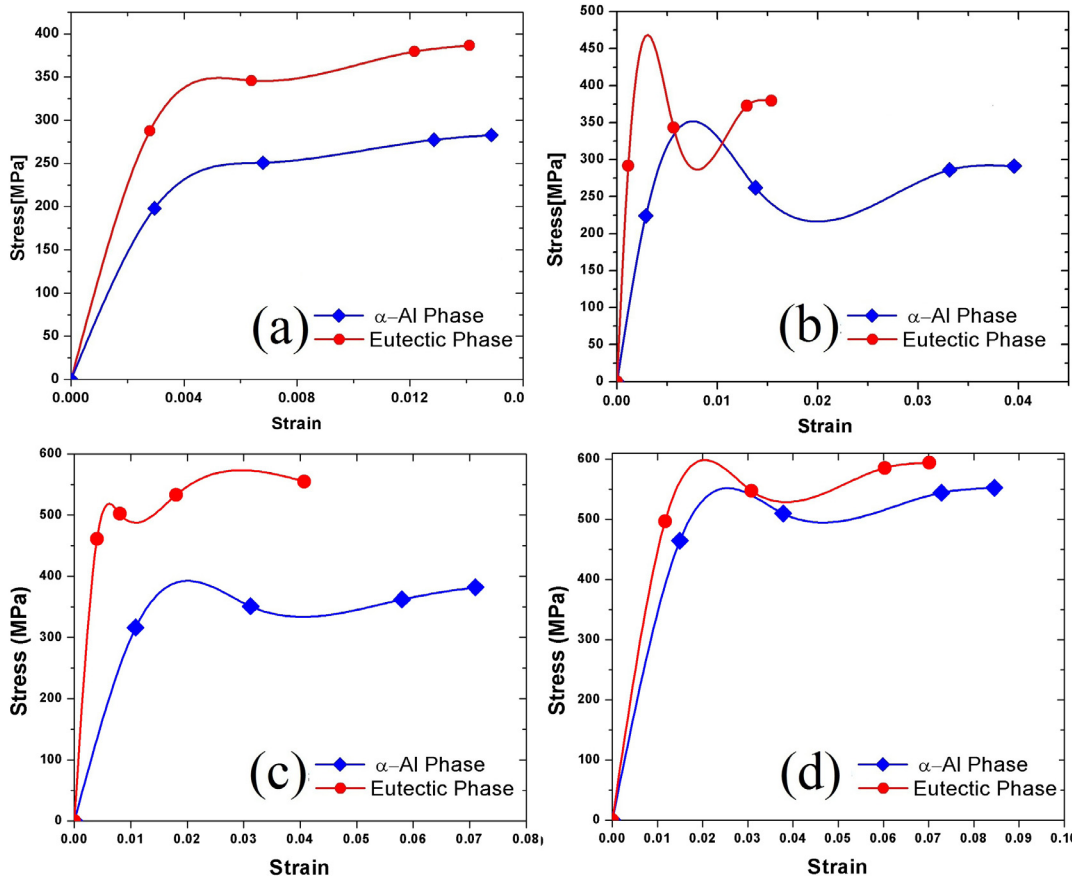Fig. 11. True stress vs. true strain plot of primary α-Al and eutectic phase with case-II boundary condition: (a) Gravity cast (P_1) (b) Gravity cast with grain refiner (P_2) (c) Rheocast (P_3) (d) SIMA (P_4)
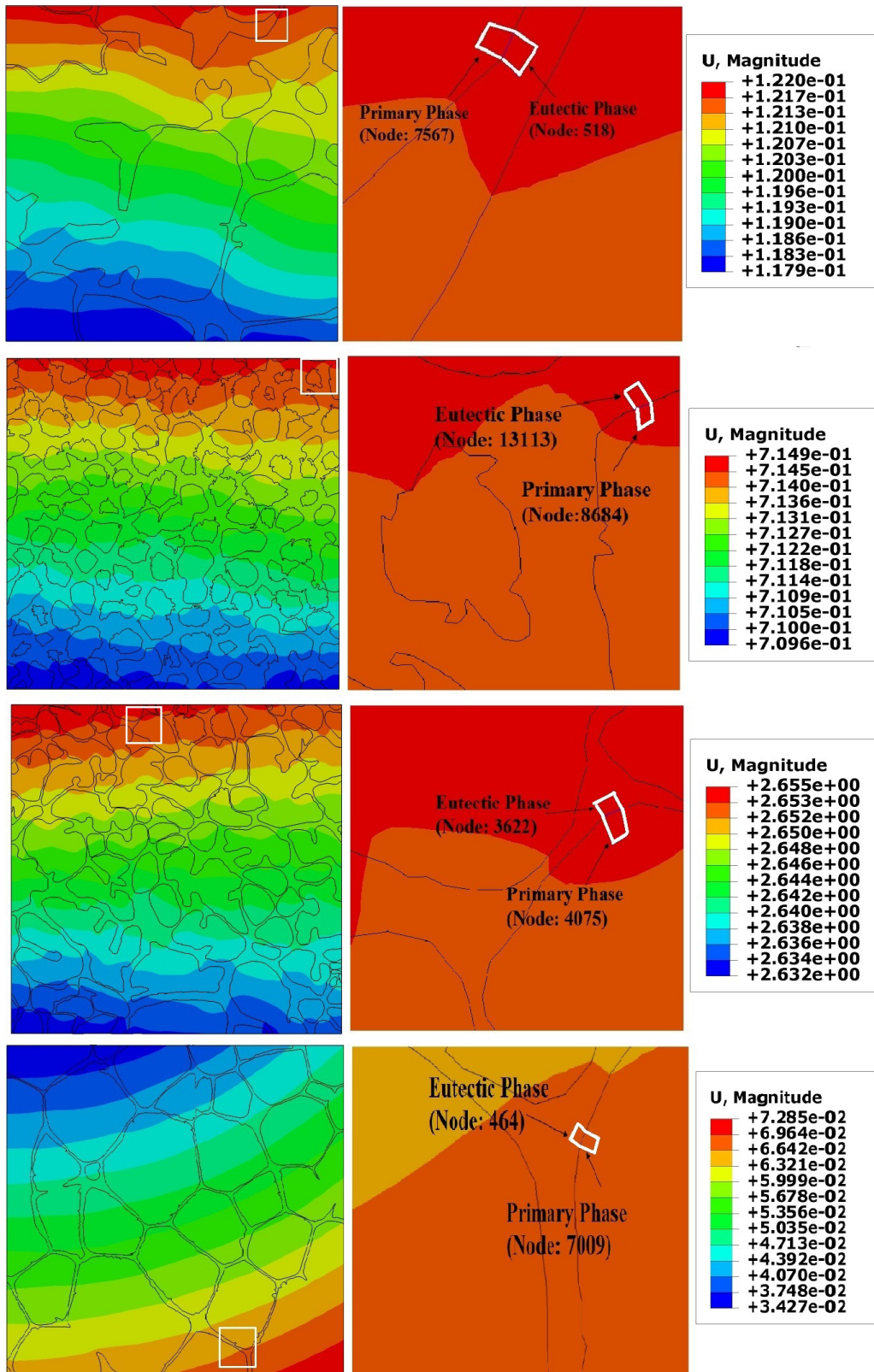
Fig. 12. Different processed RVEs and its higher magnification strain distribution of eutectic and primary α-Al phase at two neighbouring nodes with case-II boundary condition

neighbouring nodes of primary α-Al and eutectic phase is calculated from Fig. 12 and values are shown in Table 5. The Table 5 reveals that the displacement magnitude values is increased when the process shifted from P_1 to P_4, which indicates the effect of process route and condition to improve the ductility of the alloy.

This result again confirms the superiority of rheocast and SIMA process over gravity cast.

Fig. 13 shows the plastic strain of eutectic and α-Al phase of various simulated RVEs as a function of simulation step time with case-I boundary condition. It shows that how the plastic
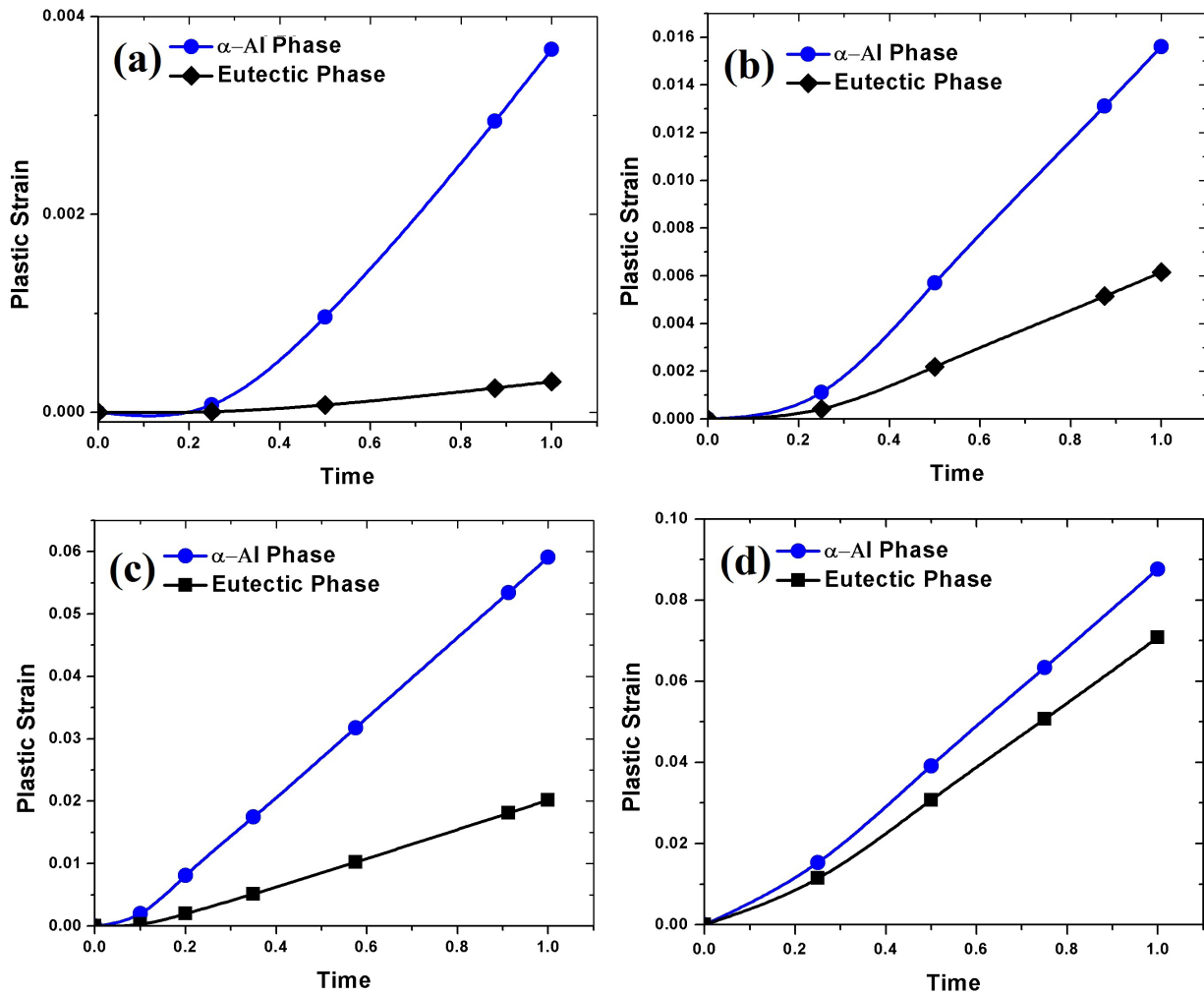
Fig. 13. Plastic strain of eutectic and α-Al phase in two adjacent nodes as a function of simulation step time with case-I boundary condition

TABLE 5

Calculated displacement magnitude of side by side node
of primary and eutectic phase under case I boundary conditions
at high strain band

Process	Primary Phase (Node No.)	Displacement (Magnitude)	Eutectic Phase (Node No)	Displacement (Magnitude)
P_1	7567	0.00367	518	0.00031
P_2	8684	0.01561	13113	0.00616
P_3	4075	0.05908	3622	0.02018
P_4	7009	0.08768	464	0.07082

strain increases with increasing load at the micro level. It is found that at the initial stage of loading the induced plastic strain is same in both the phases but when the load increases further the induced plastic strain is much higher in α-Al phase. The difference in induced plastic strain among the α-Al and eutectic phase is more in gravity cast alloy as compared to the rheocast and SIMA processed alloy due to this the gravity cast alloy possess comparatively poor mechanical properties. On the other hand, the plastic strain is increased when the process route and condition is shifted from P_1 to P_4. It again enlightens the cause of superior mechanical properties of rheocast and SIMA process alloy.

Conclusion

The micromechanical response of the Al-4.5Cu-2Mg alloy is being investigated, employing two different boundary conditions under tensile loading. Two dimensional (2D) RVEs are developed from the microstructure of gravity cast without (P_1) and with grain refiner (P_2), rheocast (P_3) and SIMA process (P_4) alloy. The simulated RVEs are analysed to understand the effect of process route and condition in terms of microstructural features on the micromechanical response using ABAQUS finite element software. The failure mode of the alloy is found to be dependent on the α-Al grain size and shape as well as eutectic and α-Al phase volume fraction. Plastic strain localization and stress concentration are occurred due to inhomogeneity in the microstructure (irregular grain). The sharp corners and narrow eutectic regions are the stress localized region and a suitable site for crack initiation. However, a sharp difference of load-carrying capacity, between the primary and eutectic phases is observed and the displacement of the primary α-Al phase node is always greater than the eutectic phase although nodes of the primary α-Al and eutectic phase lie side by side. The huge difference in induced stress and strain may be a cause for a poor mechanical response. It is found that SIMA process RVE has a better stress

and strain distribution, as the dendritic primary α-Al phase is changed to fine non-dendritic globular structure and volume fraction of eutectic phase is decreased. Therefore, major findings obtained in the present study can be useful to optimize the different process, alloy composition, and reinforcement volume fraction in alloy and composites.

REFERENCES

[1]   P. Dudek, FDM 3D Printing Technology in manufacturing composite elements, Archives of Metalurgy and Materials **58**, 1415-1418 (2013)

[2]   Z. Shan, A.M. Gokhale, Digital image analysis and microstructure modeling tools for microstructure sensitive design of materials, Int. J Plasticity **20**, 1347-1370 (2004).

[3]   V.V. Ganesh, N. Chawla, Effect of particle orientation anisotropy on the tensile behavior of metal matrix composites experiments, Mat. Sci. Eng. A **391**, 342-353 (2005).

[4]   S.K. Paul, Real microstructure based micromechanical model to simulate microstructure level deformation behavior and failure initiation in DP 590 steel, Mater. Des. **44**, 397-406 (2013).

[5]   H.T. Hossein, A. Behnam, K. Javad, S. Ghasem, Microstructural deformation pattern and mechanical behavior analyses of DP600 dual phase steel, Materials Science & Engineering A **600**, 108-121 (2014).

[6]   T. Sirinakorn, S. Wongwises, V. Uthaisangsuk, A study of local deformation and damage of dual phase steel, Materials and Design **64**, 729-742 (2014).

[7]   P. Phetlam, V. Uthaisangsuk, Microstructure based flow stress modelling for quenched and tempered low alloy steel, Materials & Design **82**, 189-199 (2015).

[8]   A. Ramazani, M. Abbasi, S. Kazemiabnavi, S. Schmauder, R. Larson, U. Prahl, Development and application of a microstructure-based approach to characterize and model failure initiation in DP steels using XFEM, Materials Science & Engineering: A **660**, 181-194 (2016).

[9]   B. Wu, N. Vajragupta, J. Lian, U. Hangen, P. Wechsuwanmanee, S. Münstermann , Prediction of plasticity and damage initiation behaviour of C45E+N steel by micromechanical modelling, Materials & Design **121**, 154-166 (2017).

[10] S.K. Paul, M. Mukherjee, Determination of bulk flow properties of a material from the flow properties of its constituent phases, Computational Materials Science 84, 1-12 (2014).

[11] C. Heinrich, M. Aldridge, A.S. Wineman, J. Kieffer, A.M. Waas, K. Shahwan, The influence of the representative volume element (RVE) size on the homogenized response of cured fiber composites, Modelling Simul. Mater. Sci. Eng. **20**, 1-25 (2012).

[12] X. Zhuang, S. Ma, Z. Zhao, Effect of particle size, fraction and carbide banding on deformation and damage behavior of ferrite–cementite steel under tensile/shear loads Modelling Simul. Mater. Sci. Eng. **25**, 1-30 (2017).

[13] T.W.J. Geus, R.H.J. Peerlings, M.G.D. Geers, Microstructural modeling of ductile fracture initiation in multi-phase materials, Engineering Fracture Mechanics **147**, 318-330 (2015).

[14] F. Farukh, L.G. Zhao, R. Jiang, P. Reed, D. Proprentner, B.A. Shollock, Realistic microstructure-based modelling of cyclic deformation and crack growth using crystal plasticity, Computational Materials Science 111, 395-405 (2016).

[15] B.S. Murty, S.A. Kori, M. Chakraborty, Grain refinement of aluminium and its alloys by heterogeneous nucleation and alloying, International Materials Reviews **47,** 3-29 (2002).

[16] E. Tzimas, A. Zavaliangos, A comparative characterization of near-equiaxed microstructures as produced by spray casting, magnetohydrodynamic casting and the stress induced, melt activated process, Materials Science and Engineering A **289**, 217-227 (2000).

[17] E.J. Lavernia, J.D. Ayers, T.S. Srivatsan, Rapid solidification processing with specific application to aluminium alloys, International Materials Reviews **37**, 1-44 (1992).

[18] A. Bolouri, M. Shahmiri, E.N. H. Cheshmeh, Microstructural Evolution during Semi-Solid State Strain Induced Melt Activation Process of Aluminium, Trans. Nonferrous Met. Soc. China **20**, 1663-1671 (2010).

[19] M.X. Xia, H.X. Zheng, S. Yuan, J.G. Li, Recrystallization of preformed AZ91D magnesium alloys in the semisolid state, Mater. Des. **26**, 343-349 (2005).

[20] A. Bolouri, M. Shahmiri, C.G. Kang, Study on the effects of the compression ratio and mushy zone heating on the thixotropic microstructure of AA 7075 aluminum alloy via SIMA process, J. Alloys Compd. **509**, 402-408 (2011).

[21] L. Sang-Yong, L. Jung-Hwan, L. Young-Seon, Characterization of Al 7075 alloys after cold working and heating in the semi-solid temperature range, J. Mater. Process. Technol. **111**, 42-47(2001).

[22] M.C. Flemings, Behaviour of Metal Alloys in the Semi-solid State, Metall. Trans. A **22,** 957-981 (1991).

[23] H.T. Jiang, Y.L. Lu, W.C. Huang, X.L. Li, M.Q. Li, Microstructural evolution and mechanical properties of the semisolid Al-4Cu-Mg alloy, Mater. Charact. **51**, 1-10 (2003).

[24] D.H. Kirkwood, Semisolid metal processing, Int. Mater. Rev. **39**, 173-189 (1994).

[25] D.M. Calin, S.J.Andersen, R. Holmestad, E. Kobayashi, T. Sato, M. Mihara, Precipitation in an Al-Mg-Cu alloy and the effect of a low amount of Ag, Materials Science & Engineering A **658**, 91-98(2016).

[26] C. Li, G. Sha, Gun, J.H. Xia, X.F. Liu, Y.Y. Wu, N. Birbilis, S.P. Ringer, N. Wu, Enhanced age-hardening response of Al-4Mg-1Cu (wt.%) microalloyed with Ag and Si Scripta Materialia **68,** 857-860 (2013).

[27] Y. Han, K. Ma, L. Li, W. Chen, H. Nagaumi, Study on microstructure and mechanical properties of Al-Mg-Si-Cu alloy with high manganese content. Materials and Design **39**, 418-424 (2012).

[28] Abaqus 6.14 Analysis User's Guide, Deformation plasticity, Dassault System, Section 23.2.13 (2014).